Journal of Histochemistry & Cytochemistry 2022, Vol. 70(7) 531–541

DOI: 10.1369/00221554221112701
journals.sagepub.com/home/jhc
SAGE

Journal of Histochemistry & Cytochemistry

Digital Staging of Hepatic Hemangiomas Reveals Spatial Heterogeneity in Endothelial Cell Composition and Vascular Senescence

Stefan Thomann, Marcell Tóth, Simon David Sprengel, Jakob Liermann, and Peter Schirmacher

Institute of Pathology (ST, MT, PS) and Department of Radiation Oncology (SDS, JL), University Hospital Heidelberg, Heidelberg, Germany, and Institute of Systems Immunology, University of Würzburg, Würzburg, Germany (ST)

Summary

Hepatic hemangioma (HH) is the most common benign primary liver tumor; however, despite its high prevalence, a stage-specific classification of this tumor is currently missing. For a spatial stage-specific classification, a tissue microarray (TMA) consisting of 98 HHs and 80 hemangioma margins and 78 distant liver tissues was digitally analyzed for the expression of 16 functional and vascular niche-specific markers. For cross-correlation of histopathology and functional characteristics, computed tomography/MRI imaging data of 28 patients were analyzed. Functional and morphological analyses revealed a high level of intra- and interpatient heterogeneity, and morphological heterogeneity was observed with regard to cellularity, vascular diameter, and endothelial cell subtype composition. While regressed hemangiomas were characterized by low blood vessel density, low beta-catenin levels, and a microvascular phenotype, non-regressed HHs showed a pronounced cellular and architectural heterogeneity. Functionally, cellular senescence–associated p16 expression identified an HH subgroup with high vascular density and increased lymphatic endothelial cell content. Histological HH regions may be grouped into spatially defined morphological compartments that may reflect the current region-specific disease stage. The stage-specific classification of HHs with signs of regression and vascular senescence may allow a better disease course–based and cell state–based subtyping of these benign vascular lesions. (J Histochem Cytochem 70. 531–541, 2022)

Keywords

continuous endothelial cells, endothelial cell heterogeneity, lymphatic endothelial cells, vascular senescence, vascular tumors

Introduction

Hepatic hemangiomas (HHs) are the most common primary tumors of the liver with a reported prevalence of approximately 2.5%.[1] HH diagnosis often occurs incidentally, and the majority of the lesions remain asymptomatic so that resection or intervention may not be required.[2] Still, a minority of HH may progress so that clinical symptoms arise and surgical resection is indicated.[3,4]

The evolution and disease stage of HH and its morphological heterogeneity may be a result of a sequence of lesion-specific alterations over time rather than a sign of disease heterogeneity itself, as analogously has been described for infantile hemangioma.[5–7] In that regard, common concepts of vascular regression that include cellular senescence of endothelial cells (ECs) are not well integrated in the study of HHs, although spontaneous regression of HHs has been described.[8,9] Moreover, common disease and EC-aging-related

Received for publication May 2, 2022; accepted June 21, 2022.

Corresponding Author:
Stefan Thomann, Institute of Pathology, University of Heidelberg, Im Neuenheimer Feld 224, 69120 Heidelberg, Germany.
E-mails: stefan.thomann@med.uni-heidelberg.de; stefan.thomann@uni-wuerzburg.de

studies strongly focus on the biology of liver sinusoidal endothelial cells (LSECs) but may not be applicable to ECs of HHs, which have a continuous endothelial cell (CEC) phenotype. So far, liver EC subtype–specific functional heterogeneity in health, aging and disease remains incompletely characterized.[10–13] Vice versa, HHs may be a good model to study cellular regression and senescence-associated changes in a hepatic CEC-specific context.

Diagnostically, typical radiographic signs that favor a diagnosis of HH include the iris diaphragm phenomenon or the light bulb sign, which are both attributable to the typical histology of HH.[14,15] While the iris diaphragm phenomenon describes the centripetal filling of contrast agent starting from the HH margin, the light bulb sign refers to the MRI hyperintensity of HH in the T2-weighted sequence. Depending on the histological type and degree of regression, a cross-correlation of vascular histomorphology and related radiomorphological phenotype is possible.[15,16] Yet, a high-resolution and high-throughput tissue-based analysis to study the correlation between regression and immunohistochemical marker expression in HHs is missing.

The following study aims to highlight the morphological and functional heterogeneity of HHs by MRI/computed tomography (CT) scan images and characterize these lesions using digital image analysis. New morphological and phenotypic markers are identified, which may enhance HH characterization according to the current cell state and spatial disease stage, which may improve the understanding of the sequence of molecular processes in vascular regression in a liver CEC-specific context.

Materials and Methods

Tissue Microarray Design and Patient Cohort

HHs included in this analysis (n=98) were resected from 1995 to 2017 at the Department of Surgery, University Hospital Heidelberg. Samples were provided by the Tissue Bank of the National Center for Tumor Diseases (NCT) Heidelberg, Germany, in accordance with the regulations of the tissue bank and the approval of the ethics committee of Heidelberg University (application number S-230/20).

The female HH specimens (n=64) were resected with an age of 54.8 ± 14.1 (SD) years and a lesion size of 5.6 ± 5.5 cm. Male patient HH specimens (n=34) were resected with an age of 59.1 ± 11.5 years and a lesion size of 5.4 ± 5.5 cm. To address potential inter- and intralesional heterogeneity within HHs, a large core (1.5 mm core size) TMA was generated, consisting of four cores per specimen when sufficient sampling was possible (two cores to assess hemangioma center, and one core each to assess hemangioma margin and far distant liver tissue). In total, the TMA consisted of 339 cores (n=181 hemangioma, n=80 margin, n=78 liver).

Slide Scanning, Quantification of Vessel Diameter, Positive Cell Detection, Antibodies and Statistics

TMAs were scanned using an Aperio AT2 scanning device (Leica; Wetzlar, Germany) with a resolution of 0.25 µm and 40×-fold magnification. For accurate cell detection, quantification, and cell type annotation of immunohistochemical stainings, the TMA dearrayer algorithm within QuPath was used.[17] Cores with artifacts (overlay/tears) or cores missing more than one third of the tissue area were manually excluded. The average diameter of hemangioma vessels was evaluated in cores with an annotation of "hemangioma center" by measuring the diameter of five representative vessels using the line tool. Cell detection was performed based on optical density sum with a set pixel size of 0.5 µm. For automated image quantification of nuclear or cytoplasmic stainings, the TMA dearrayer was used after an image normalization step and single thresholding. Stainings were then quantified using the integrated inbuilt object counter tool within the TMA dearrayer and further analyzed in Excel and R studio. In total, 16 immunohistochemical markers were stained to assess EC content and subtype (CD31, THBD (thrombomodulin), CD34, FVIII, ERG, PDPN (podoplanin)), cellular environment (CD68, DES), cell cycle state (Ki67, p16, p53, CDK4) and responsiveness to extracellular cues/pathway activity (CATB, MET, MYC, BRAFV600E). A complete list of all antibodies and dilutions used can be found in Table 1.

Shapiro–Wilk test was used to test for normality. Wilcoxon rank-sum test was used for calculating p-values of non-normally distributed datapoints. Benjamini and Hochberg correction was applied to correct for multiple testing while simultaneously avoiding overcorrection of p-values (p-adjust function, R studio). P values are indicated as follows: *p<0.05, **p<0.01, ***p<0.001. Plots were generated in Excel and R studio (ggplot2 and ggpubr).

Additional methods used in this study are compiled in the supplemental materials and methods section.

Results

HHs Are Characterized by a Heterogeneous Contrast Agent Uptake and Degree of Tissue Regression

To study vascular flow as a functional parameter in HH, we first analyzed CT/MRI scans of 28 patients. In

Table 1. Antibody List.

Antibody	Clone	Company / Order Number	Dilution
BRAF V600E	VE1	Ventana Medical Systems #760-5095	—
CD31	JC70	Ventana Medical Systems #760-4378	—
CD34	QBEnd/10	Ventana Medical Systems #760-2927	—
CD68	PG-M1	DAKO #M0876	1:100
CDK4	DCS-31	Life Technologies #AHZ0202	1:50
C-MET	SP44	Ventana Medical Systems #790-4430	—
C-MYC	Y69	Ventana Medical Systems #790-4628	—
CTNNB1	14	Ventana Medical Systems #760-4242	—
DESMIN	DE-R-11	Ventana Medical Systems #760-2513	—
D2-40 (PDPN)	D2-40	Cell Marque #760-4395	—
ERG	EPR3864	Ventana Medical Systems #790-4576	—
FVIII	polyclonal	Ventana Medical Systems #760-2642	—
Ki-67	30-9	Ventana Medical Systems #05278384001	—
p16	MX007	Zeta Corporation #Z2016	1:100
p53	DO-7	DAKO #M7001	1:400
THBD	1009	DAKO #M0617	1:40

multiple large hemangiomas, so-called giant hemangiomas,[18] region-specific differences in the uptake of contrast agent were detected (Fig. 1A). To display this inhomogeneity at higher resolution, three-dimensional reconstructions and limited density range pixel visualizations of a hemangioma margin in native and venous phases were generated, which confirmed inhomogeneous uptake of contrast agent (Fig. 1B). Moreover, single-plane surface plot visualizations confirmed phase-specific heterogeneity of density values in the lesion (Fig. 1C). As these functional differences in vascular flow and contrast agent uptake may be due to differences in tissue composition, we next analyzed resected HHs using conventional histology. To assess the degree of hemangioma regression independent of histological subtype, 63 hemangiomas were evaluated using H&E whole slides. As expected, the majority of hemangiomas showed varying signs of regression, and in 20% of HHs regression was scored as "very strong" (Fig. 1D and E). Histology revealed architectural differences in individual patients and within large lesions with a coexistence of non-regressed, partially regressed, and fully regressed areas (Fig. 1E).

In conclusion, CT/MRI scans and H&E sections confirmed functional and architectural differences and heterogeneity in HHs.

Immunohistochemical Characterization of HH Reveals Endothelial Cell Heterogeneity

To analyze morphological and expression differences of HHs on a large scale in a spatial context, a single institutional TMA was generated that contained 98 HHs, 80 margins, and 78 adjacent liver tissues, which were stained for 16 markers (Fig. 1F and G; Supplemental Fig. 1A; Table 1). To assess EC content, positive cell detection of CD31, THBD, CD34, factor VIII–related antigen (FVIII), and ETS transcription factor ERG (ERG) was performed (Fig. 2A). These markers stained ECs of HH homogeneously, while in adjacent liver tissues CD31, THBD, CD34, and FVIII were mainly expressed in ECs of the portal tract, whereas LSECs were weakly positive (CD31, THBD, FVIII) or negative (CD34). Nuclear staining for ERG selectively stained LSEC and CEC nuclei, as previously described.[19,20] To correlate overall EC cellularity within cores, a correlation analysis of ERG-positive nuclei and CD31-, THBD-, CD34-, and FVIII-positive cells was performed (Supplemental Fig. 1B). The high positive correlations of the previously described markers confirmed a CEC phenotype in HHs and demonstrated an accurate cell estimation by the marker panel being used.[21]

Next, to test for CEC heterogeneity in HHs, we stained for the lymphatic EC (lyEC) marker PDPN. Indeed, in 90.6% of analyzed HH cores, $PDPN^+$ lyECs could be observed next to PDPN-negative ECs (Fig. 2B). After setting a higher cut-off value for $PDPN^+$ cells, a total of 77% of HH center cores still contained lyEC. In average, 1.14% of all cells were detected as $PDPN^+$; however, the number of $PDPN^+$ cells was increased up to 18.48%. Digitally aligned consecutive sections of H&E, CD31, ERG, and PDPN revealed that these $PDPN^+$ cells were ERG^+ $CD31^+$ (Fig. 2C). Core-specific cell detection revealed an increase in positive cells from distant liver, HH margin, to HH center for all EC markers (Fig. 2D). The number of $CD68^+$

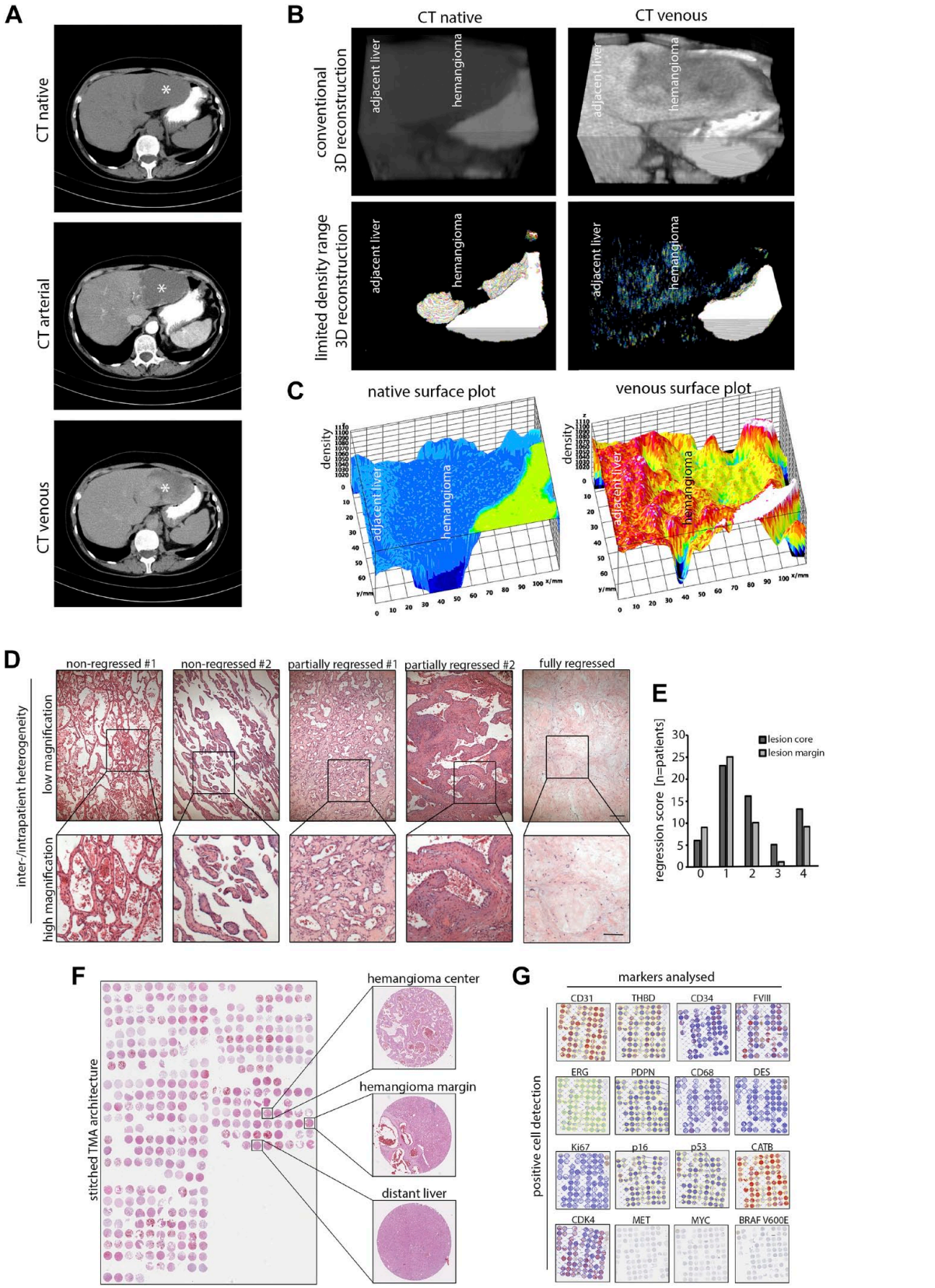

Figure 1. *(continued)*

Figure 1. Functional and morphological heterogeneity in HHs and study design. (A) CT scan of a patient with a large hemangioma located in the left liver lobe (asterisk). Specified imaging phases show an inhomogeneous uptake of contrast agent in the lesion. (B) Three-dimensional reconstruction of the hemangioma margin of the same patient. Limited density range visualization removes liver-specific signal and visualizes inhomogeneous uptake of contrast agent in HH. (C) Native and venous phase density surface plots of the same patient. Inhomogeneous contrast agent uptake in the lesion can be observed. (D) H&E images of five HHs with different intralesional morphology as displayed by vascular morphology and degree of tissue regression. Scale bar: 200 μm (low) and 100 μm (high). (E) Distribution of the regression score in HH centers and marginal zones (0 = "none," 1 = "slight," 2 = "intermediate," 3 = "strong," 4 = "very strong"; *n*=63). (F) Stitched H&E overview of the TMA consisting of five slides in total covering 98 HH, 80 HH margins, and 78 distant liver tissues and 339 cores in total. (G) Low magnification overview of a tissue microarray section after positive cell detection of the respective marker panel used in this study (see Table 1). MET, MYC, and BRAF V600E were not digitally scored due to negative staining results. Abbreviations: HH, hepatic hemangioma; CT, computed tomography; H&E, hematoxylin and eosin; TMA, tissue microarray.

cells was significantly reduced in both HH margin and HH center compared with distant liver (Supplemental Fig. 2A and B). Desmin$^+$ (DES) cells were significantly enriched in HH margins but not in HH centers (Supplemental Fig. 2A and B).

Together, the first characterization of HHs and distant liver tissues revealed heterogeneity in CEC subtype composition and cellular microenvironment.

A Subset of HHs Is Identified as p16-senescent

With the aim to functionally subtype HHs, p16 expression was analyzed as a common marker of cellular senescence.[22,23] A total of 90.9% of HH cores contained p16$^+$ cells. In average, a p16$^+$ cell count of 7.4% was observed, with the percentage of positive cells ranging up to 38.7%. To further classify p16^{high} and p16^{low} lesions, a cutoff of 10% was chosen, which is within the expected range of positive cells in models of cellular senescence (Fig. 3A).[23] To compare the marker expression of non-senescent (p16^{low}) and p16-senescent (p16^{high}) HHs with strongly regressed lesions, fully regressed HHs were also included in our classification strategy. Both p16-senescent and regressed HHs represented 12% and 8% in our cohort compared with 80% of non-senescent HHs (Fig. 3B). Except for one core, regression and p16-senescence were mutually exclusive traits. To functionally validate the cellular senescence in HH ECs, p53 stainings were analyzed, which is another common marker of senescence.[24] Indeed, the correlation analysis of p16$^+$ cells and p53$^+$ cells validated cellular senescence in HHs using an independent senescence marker ($r_S = 0.42$, ***$p<0.001$; Fig. 3C and D), and the positive correlation of two independent senescence markers indicated the existence of HHs with low or high numbers of senescent cells.

p16-senescent HHs showed significantly higher EC density (measured by ERG$^+$) and lyEC content (PDPN$^+$; Fig. 4A). The same trend was observed for CD34$^+$ cell numbers between p16-senescent and non-senescent HHs, however not reaching the level of significance (Fig. 4A). Regressed HHs were characterized by low numbers of CD31$^+$, CD34$^+$, ERG$^+$, and PDPN$^+$ cells and reduced vascular diameters (Fig. 4A). Ki67$^+$ cells were lower in regressed HHs, but there was no significant difference in Ki67 positivity between p16-senescent and non-senescent hemangiomas (Fig. 3D and 4A). Also, "macroscopic size" and "age at resection" as clinical parameters were not significantly different in a core-specific HH comparison, but there was a trend toward smaller average lesion size for p16-senescent HH cores compared with regressed HH (Fig. 4B; p=0.1). Finally, the intrapatient region-specific stage subclassification was compared in patients, where multiple hemangioma cores have been assessed. While in 76% cores were monotypically classified, in 24% a heterotypic stage pattern as a sign of spatially restricted differences within HH tissue was observed between cores of the same patient. The majority of intrapatient heterogeneity was based on senescent/non-senescent (59%) and non-senescent/regressed stages (35%).

In conclusion, a digitally assisted staging revealed morphological, functional, and intralesional differences in HH cores regarding EC composition, the presence of vascular senescence, and HH regression.

Hemangioma Regression Is Associated With Reduced Macrophage Infiltration and Beta-catenin Expression

As several HH cores showed signs of cellular senescence, we stained for the expression of p16-regulated downstream targets. On the protein level, one common p16-regulated protein is cyclin-dependent kinase 4 (CDK4), which forms complexes with cyclin D that are essential for cell-cycle progression.[25] Indeed, ubiquitous CDK4 expression in HHs was detected independent of the disease stage (Fig. 4C). Previously, catenin beta 1 (CATB encoded by CTNNB1 gene) has been described as a downstream effector of ERG, CATB thereby promoting vascular stability and angiogenesis.[26] To evaluate whether CATB expression in HHs correlates with a regression-free stage, positive

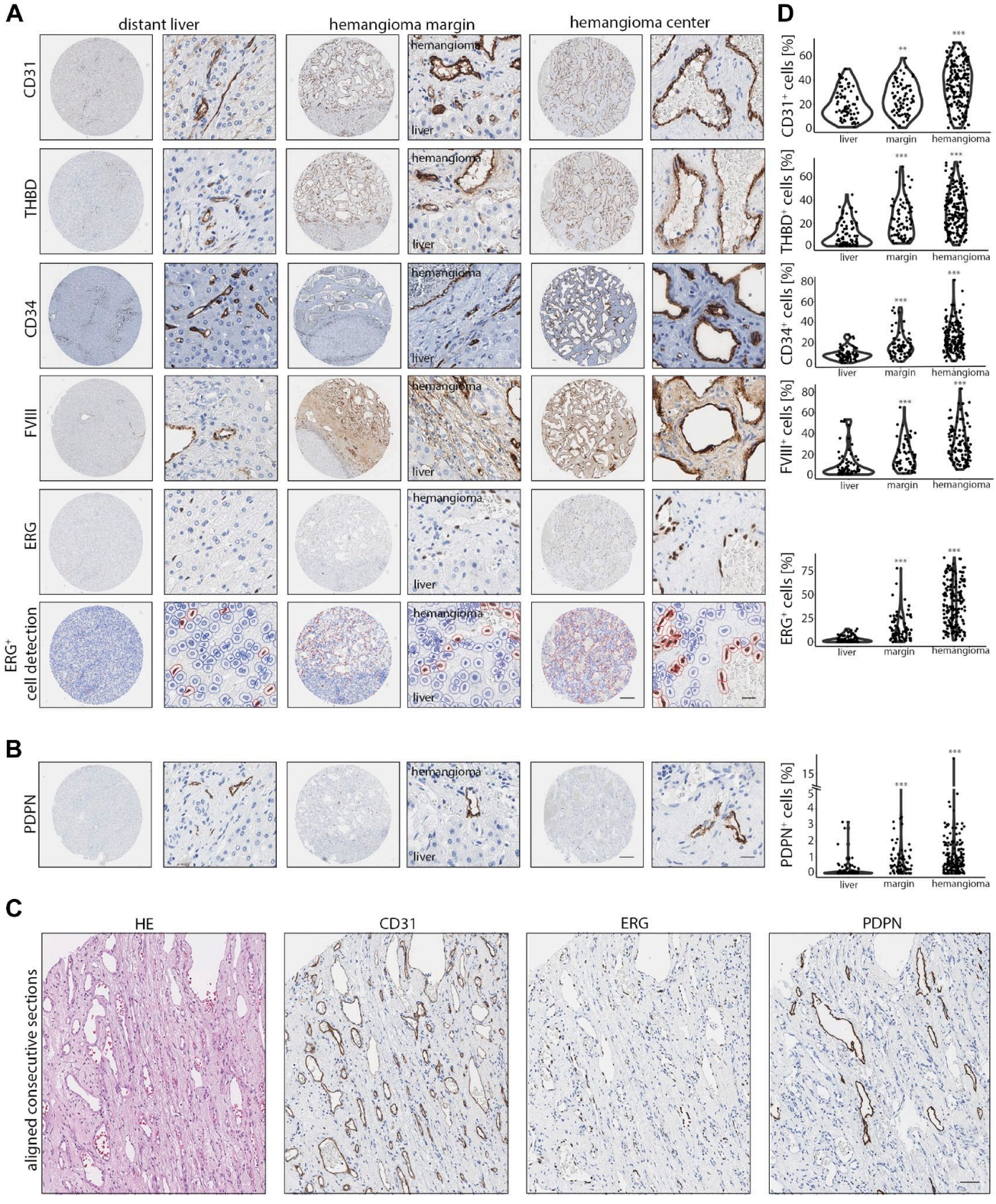

Figure 2. *(continued)*

Figure 2. A CEC marker panel reveals endothelial heterogeneity in HHs. (A) Low and high magnification of CD31, THBD, CD34, FVIII, and ERG in liver, hemangioma margin, and hemangioma center. Last row: Overlay of ERG-positive cell detection demonstrates a highly accurate cell classification. Scale bar: 250 µm (low) and 20 µm (high). (B) Low and high magnification of PDPN expression in liver, hemangioma margin, and hemangioma center. In liver, only a minor fraction of portal vessels stain positive for PDPN, whereas a higher abundance of $PDPN^+$ ECs in hemangioma margins and centers can be detected. Scale bar: 250 µm (low) and 20 µm (high). (C) Aligned consecutive H&E and immunohistochemical sections of CD31, ERG, and PDPN of HH. The presence of $PDPN^+$ lyECs next to $CD31^+$ and ERG^+ cells demonstrates intralesional vascular heterogeneity. Scale bar: 100 µm. (D) Percentual distribution of $CD31^+$, $THBD^+$, $CD34^+$, $FVIII^+$, ERG^+, and $PDPN^+$ cells in liver, hemangioma margin (margin), and hemangioma center (hemangioma). Comparison of liver tissue vs tissue area of interest by Wilcoxon rank-sum test (**$p<0.01$, ***$p<0.001$). Abbreviations: CEC, continuous endothelial cell; HH, Hepatic hemangioma; FVIII, factor FVIII related antigen; ERG, ETS transcription factor ERG; PDPN, podoplanin; EC, endothelial cell; H&E, haematoxylin eosin; lyEC, lymphatic endothelial cell; THBD, thrombomodulin.

cell detection was performed. Although no significant differences in the distribution of $CATB^+$ cells was found between p16-senescent and non-senescent HHs, a significant reduction in $CATB^+$ cells in regressed HH cores was observed (Fig. 4C and D). Next, MET Proto-Oncogene (MET) and MYC Proto-Oncogene (MYC) as markers of proliferative and migratory angiogenesis were screened.[21,27] Interestingly, both markers were not expressed in HHs (Supplemental Fig. 3A). BRAF mutations at hotspot codon V600 have recently been identified in a cohort of human HHs.[28] This prompted us to screen for the common BRAF V600E mutation in our cohort. However, all HHs of our cohort were negative for BRAF V600E (Supplemental Fig. 3A). Finally, regressed hemangioma cores showed a reduced macrophage content as measured by $CD68^+$ cells compared with p16-senescent HHs, whereas DES^+ cells were equally distributed in HH subtypes (Fig. 4C and D; Supplemental Fig. 3B and C).

In summary, these results suggest a role of early p16-mediated vascular senescence in HHs with preserved CATB expression that is lost in fully regressed HHs.

Discussion

The low risk of disease progression and the infrequent necessity to resect HHs result in a relative lack of knowledge regarding tissue morphology, marker expression, and lesion-specific evolution over time, although HH may serve as a suitable model to study EC subtype-specific mechanisms of vascular regression in a CEC-specific context. In case of HH resection, tissue acquisition is biased toward highly progressed, large, and morphologically heterogeneous hemangiomas that may already show the full spectrum of senescence-associated changes and tissue regression. This collection bias, which is also present in our cohort, may affect the understanding of how these lesions develop over time. To address this problem, we here generated a large single-center cohort of 98 HHs and analyzed tissues in a core-specific manner so that individual cores contained a uniform morphology. This strategy allowed to better understand the evolution of HHs over time on a broader scale and allowed the subclassification of spatially restricted HH disease stages. For example, in our cohort, both lymphatic and vascular ECs of HH showed significant differences in cell numbers when comparing non-senescent (80%), p16-senescent (12%), and regressed lesions (8%), indicating that both EC compartments may undergo a sequential evolution of EC expansion that leads to cell density–induced senescence and/or regression. A comparable concept of HH evolution and regression has been proposed for infantile hemangioma.[5,7] Unfortunately, Ki67 proliferation indices in our cohort were low and showed a stochastic pattern so that it did not qualify as an early disease stage discriminator. This was in accordance with the average HH size and patient age that excluded early-onset disease. Using a randomly punched two-core TMA classification strategy, we could identify 76% of HHs with a spatial monotypic and 24% with a heterotypic disease stage, which demonstrates intralesional stage-specific differences in advanced lesions. Future studies, which simultaneously analyze more than two HH lesional compartments and quantify the overall predominant stage, are required to deeply characterize the spatial heterogeneity within HHs and to perform meaningful clinicopathological correlations.

Senescence-associated marker expression revealed that apart from morphological criteria, an analysis of p16-expression may provide insight into hemangioma-"stage" as it may have potential to biologically predict the tendency toward regression in spatially defined HH tissue compartments. As such, it would be interesting to investigate whether the soluble factors of the senescence-associated secretome would differ between the HH subgroups proposed here.[29] The microenvironment has long been discussed as one potential contributing factor in the development and progression of HHs.[30,31] For example, the role of endogenous and exogenous estrogen has been found to increase the HH size in a minority of patients.[32] Focusing on the cell-specific microenvironment, the role of macrophages has been studied in infantile

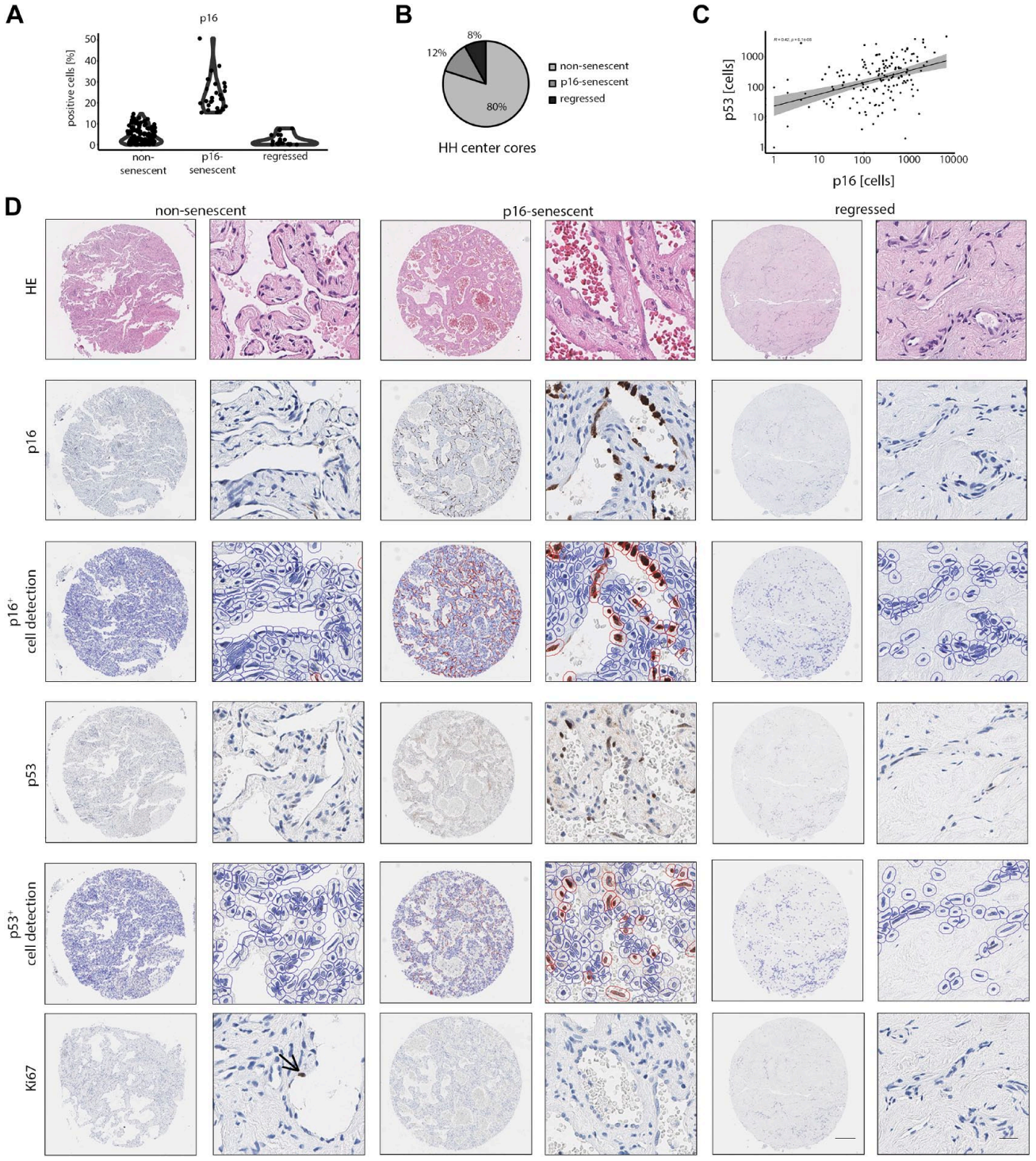

Figure 3. Defined spatial- and core-specific stages of non-senescent, p16-senescent, and regressed HHs. (A) Percentual distribution of $p16^+$ cells in non-senescent, p16-senescent, and regressed hemangiomas after digital senescence classification. Cutoff for p16-positivity was set to 10%. (B) Percentual distribution of non-senescent, p16-senescent, and regressed hemangiomas after HH classification. (C) Correlation analysis between $p16^+$ and $p53^+$ cell numbers in HH cores (Spearman correlation analysis). (D) Low and high magnification of H&E, p16, $p16^+$ cell detection, p53, $p53^+$ cell detection, and Ki67 in non-senescent, p16-senescent, and regressed hemangiomas. Arrow indicates a $Ki67^+$ EC in a non-senescent HH. Scale bar: 250 µm (low) and 20 µm (high). Abbreviations: HH, hepatic hemangioma; H&E, haematoxylin eosin; EC, endothelial cell.

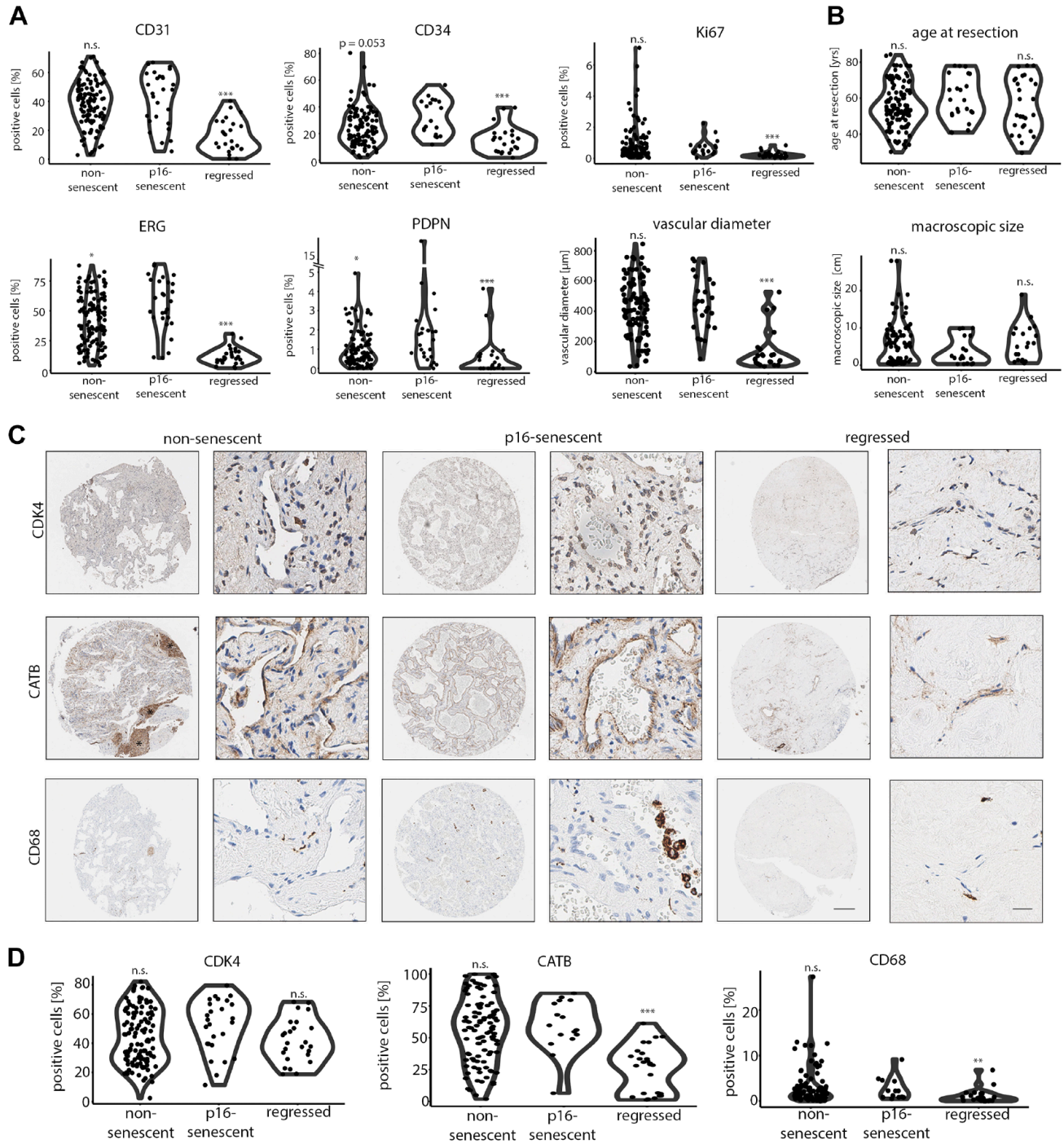

Figure 4. Unique cell composition in non-senescent, p16-senescent, and regressed HHs. (A) Percentual distribution of $CD31^+$, $CD34^+$, ERG^+, $PDPN^+$, and $Ki67^+$ cells and average vascular diameters in non-senescent, p16-senescent, and regressed hemangiomas after HH classification. Comparison of p16-senescent hemangiomas vs subgroup of interest by Wilcoxon rank-sum test (*$p<0.05$, ***$p<0.001$). (B) Age at resection and HH macroscopic size in non-senescent, p16-senescent, and regressed hemangiomas. Comparison of p16-senescent hemangiomas vs subgroup of interest by Wilcoxon rank-sum test (n.s.). (C) Low and high magnification of CDK4, CATB, and CD68 in non-senescent, p16-senescent, and regressed hemangiomas. Scale bar: 250 µm (low) and 20 µm (high). Asterisk (*) demarcates insulas of CATB-positive retained hepatocytes in a non-senescent HH. (D) Percentual distribution of $CDK4^+$, $CATB^+$, and $CD68^+$ cells in non-senescent, p16-senescent, and regressed hemangiomas after HH classification. Comparison of p16-senescent hemangiomas vs subgroup of interest by Wilcoxon rank-sum test (**$p<0.01$, ***$p<0.001$). Abbreviations: HH, hepatic hemangioma; CDK4, cyclin-dependent kinase 4; CATB, catenin beta 1; n.s., not significant.

hemangioma where it was proposed to contribute to the proliferation and regression of these lesions.[33] For instance, C-C motif chemokine ligand 2 has been shown to be associated with the recruitment of macrophages in hepatic neoplastic disease and is known to be expressed by interstitial macrophages and smooth muscle cells in infantile hemangioma.[34,35] A reduction of macrophage numbers in fully regressed lesions observed in our cohort may thus correlate with a biological role of these cells in HH evolution.

Altogether, a high-throughput spatial TMA-based HH disease staging into non-senescent, p16-senescent, and regressed lesions revealed morphological, functional, intralesional, and marker-specific differences.

Acknowledgments

The authors thank Nina Wilhelm, Veronika Eckel, and Alexander Brobeil (NCT Tissue Bank and Institute of Pathology, University Hospital Heidelberg) for their support.

Competing Interests

The author(s) declared no potential conflicts of interest with respect to the research, authorship, and/or publication of this article.

Author Contributions

ST helped with the conception and design of the study; ST, MT, SDS, and JL with the acquisition and analysis of data; ST and PS with the drafting the manuscript and the figures; and PS with supervision. All authors have read and approved the final manuscript.

Funding

The author(s) received no financial support for the research, authorship, and/or publication of this article.

Ethics Approval Statement

All analyses have been approved by the Ethics Committee of the University of Heidelberg (application number S-230/20).

Access to Tissue Microarray Material

The tissue microarray is stored at the Tissue Bank of the National Center for Tumor Diseases (NCT) Heidelberg. For material requests, contact the corresponding author.

Literature Cited

1. Mocchegiani F, Vincenzi P, Coletta M, Agostini A, Marzioni M, Baroni GS, Giovagnoni A, Guerrieri M, Marmorale C, Risaliti A, Vivarelli M. Prevalence and clinical outcome of hepatic haemangioma with specific reference to the risk of rupture: a large retrospective cross-sectional study. Dig Liver Dis. 2016;48:309–14.
2. Furumaya A, van Rosmalen BV, Takkenberg RB, van Delden OM, Dejong CHC, Verheij J, van Gulik TM. Transarterial (chemo-)embolization and lipiodolization for hepatic haemangioma. Cardiovasc Intervent Radiol. 2019;42:800–11.
3. Farges O, Daradkeh S, Bismuth H. Cavernous hemangiomas of the liver: are there any indications for resection? World J Surg. 1995;19:19–24.
4. Toro A, Mahfouz AE, Ardiri A, Malaguarnera M, Malaguarnera G, Loria F, Bertino G, Di Carlo I. What is changing in indications and treatment of hepatic hemangiomas. A review. Ann Hepatol. 2014;13:327–39.
5. Ritter MR, Moreno SK, Dorrell MI, Rubens J, Ney J, Friedlander DF, Bergman J, Cunningham BB, Eichenfield L, Reinisch J, Cohen S, Veccione T, Holmes R, Friedlander SF, Friedlander M. Identifying potential regulators of infantile hemangioma progression through large-scale expression analysis: a possible role for the immune system and indoleamine 2,3 dioxygenase (IDO) during involution. Lymphat Res Biol. 2003;1:291–9.
6. Takahashi K, Mulliken JB, Kozakewich HP, Rogers RA, Folkman J, Ezekowitz RA. Cellular markers that distinguish the phases of hemangioma during infancy and childhood. J Clin Invest. 1994;93:2357–64.
7. Leaute-Labreze C, Harper JI, Hoeger PH. Infantile haemangioma. Lancet. 2017;390:85–94.
8. Erusalimsky JD. Vascular endothelial senescence: from mechanisms to pathophysiology. J Appl Physiol (1985). 2009;106:326–32.
9. Aydin O, Acunas B, Poyanli A, Serin KR, Ibis C, Ozden I. Spontaneous regression of liver hemangiomas: a single-institution analysis of 46 patients. Eur J Gastroenterol Hepatol. 2021;33:1436–40.
10. Aird WC. Phenotypic heterogeneity of the endothelium: II. Representative vascular beds. Circ Res. 2007;100:174–90.
11. Maeso -Diaz R, Ortega-Ribera M, Fernandez-Iglesias A, Hide D, Munoz L, Hessheimer AJ, Vila S, Frances R, Fondevila C, Albillos A, Peralta C, Bosch J, Tacke F, Cogger VC, Gracia-Sancho J. Effects of aging on liver microcirculatory function and sinusoidal phenotype. Aging Cell. 2018;17:e12829.
12. Gracia-Sancho J, Caparros E, Fernandez-Iglesias A, Frances R. Role of liver sinusoidal endothelial cells in liver diseases. Nat Rev Gastroenterol Hepatol. 2021;18:411–31.
13. Thomann S, Baek S, Ryschich E. Impact of wall shear stress and ligand avidity on binding of anti-CD146-coated nanoparticles to murine tumor endothelium under flow. Oncotarget. 2015;6:39960–8.
14. Mamone G, Miraglia R. The “light bulb sign” in liver hemangioma. Abdom Radiol (NY). 2019;44:2327–8.
15. Klotz T, Montoriol PF, Da Ines D, Petitcolin V, Joubert-Zakeyh J, Garcier JM. Hepatic haemangioma: common and uncommon imaging features. Diagn Interv Imaging. 2013;94:849–59.
16. Vilgrain V, Boulos L, Vullierme MP, Denys A, Terris B, Menu Y. Imaging of atypical hemangiomas of the liver with pathologic correlation. Radiographics. 2000;20:379–97.

17. Bankhead P, Loughrey MB, Fernandez JA, Dombrowski Y, McArt DG, Dunne PD, McQuaid S, Gray RT, Murray LJ, Coleman HG, James JA, Salto-Tellez M, Hamilton PW. QuPath: open source software for digital pathology image analysis. Sci Rep. 2017;7:16878.
18. Choi BI, Han MC, Park JH, Kim SH, Han MH, Kim CW. Giant cavernous hemangioma of the liver: CT and MR imaging in 10 cases. AJR Am J Roentgenol. 1989;152: 1221–6.
19. Birdsey GM, Dryden NH, Amsellem V, Gebhardt F, Sahnan K, Haskard DO, Dejana E, Mason JC, Randi AM. Transcription factor Erg regulates angiogenesis and endothelial apoptosis through VE-cadherin. Blood. 2008;111:3498–506.
20. Shah AV, Birdsey GM, Peghaire C, Pitulescu ME, Dufton NP, Yang Y, Weinberg I, Osuna Almagro L, Payne L, Mason JC, Gerhardt H, Adams RH, Randi AM. The endothelial transcription factor ERG mediates Angiopoietin-1-dependent control of Notch signalling and vascular stability. Nat Commun. 2017;8:16002.
21. Thomann S, Weiler SME, Marquard S, Rose F, Ball CR, Toth M, Wei T, Sticht C, Fritzsche S, Roessler S, De La Torre C, Ryschich E, Ermakova O, Mogler C, Kazdal D, Gretz N, Glimm H, Rempel E, Schirmacher P, Breuhahn K. YAP orchestrates heterotypic endothelial cell communication via HGF/c-MET signaling in liver tumorigenesis. Cancer Res. 2020;80:5502–14.
22. Rayess H, Wang MB, Srivatsan ES. Cellular senescence and tumor suppressor gene p16. Int J Cancer. 2012;130:1715–25.
23. Baker DJ, Childs BG, Durik M, Wijers ME, Sieben CJ, Zhong J, Saltness RA, Jeganathan KB, Verzosa GC, Pezeshki A, Khazaie K, Miller JD, van Deursen JM. Naturally occurring p16(Ink4a)-positive cells shorten healthy lifespan. Nature. 2016;530:184–9.
24. Rufini A, Tucci P, Celardo I, Melino G. Senescence and aging: the critical roles of p53. Oncogene. 2013; 32:5129–43.
25. Sheppard KE, McArthur GA. The cell-cycle regulator CDK4: an emerging therapeutic target in melanoma. Clin Cancer Res. 2013;19:5320–8.
26. Birdsey GM, Shah AV, Dufton N, Reynolds LE, Osuna Almagro L, Yang Y, Aspalter IM, Khan ST, Mason JC, Dejana E, Gottgens B, Hodivala-Dilke K, Gerhardt H, Adams RH, Randi AM. The endothelial transcription factor ERG promotes vascular stability and growth through Wnt/beta-catenin signaling. Dev Cell. 2015;32: 82–96.
27. Testini C, Smith RO, Jin Y, Martinsson P, Sun Y, Hedlund M, Sainz-Jaspeado M, Shibuya M, Hellstrom M, Claesson -Welsh L. Myc-dependent endothelial proliferation is controlled by phosphotyrosine 1212 in VEGF receptor-2. EMBO Rep. 2020;21:e50409.
28. Janardhan HP, Meng X, Dresser K, Hutchinson L, Trivedi CM. KRAS or BRAF mutations cause hepatic vascular cavernomas treatable with MAP2K-MAPK1 inhibition. J Exp Med. 2020;217:e20192205.
29. Coppe JP, Desprez PY, Krtolica A, Campisi J. The senescence-associated secretory phenotype: the dark side of tumor suppression. Annu Rev Pathol. 2010;5: 99–118.
30. Mahajan D, Miller C, Hirose K, McCullough A, Yerian L. Incidental reduction in the size of liver hemangioma following use of VEGF inhibitor bevacizumab. J Hepatol. 2008;49:867–70.
31. Wang Z, Yuan Y, Zhuang H, Jiang R, Hou J, Chen Q, Zhang F. Hepatic haemangiomas: possible association with IL-17. J Clin Pathol. 2012;65:146–51.
32. Glinkova V, Shevah O, Boaz M, Levine A, Shirin H. Hepatic haemangiomas: possible association with female sex hormones. Gut. 2004;53:1352–5.
33. Wu KQ, Muratore CS, So EY, Sun C, Dubielecka PM, Reginato AM, Liang OD. M1 macrophage-induced endothelial-to-mesenchymal transition promotes infantile hemangioma regression. Am J Pathol. 2017;187: 2102–11.
34. Thomann S, Weiler SME, Wei T, Sticht C, De La Torre C, Toth M, Rose F, Tang Y, Ritz T, Ball C, Glimm H, Ryschich E, Schirmacher P, Breuhahn K. YAP-induced Ccl2 expression is associated with a switch in hepatic macrophage identity and vascular remodelling in liver cancer. Liver Int. 2021;41:3011–23.
35. Isik FF, Rand RP, Gruss JS, Benjamin D, Alpers CE. Monocyte chemoattractant protein-1 mRNA expression in hemangiomas and vascular malformations. J Surg Res. 1996;61:71–6.